A 3D MRI-Based Cardiac Computer Model to Study Arrhythmia and Its In-vivo Experimental Validation

Mihaela Pop[1], Maxime Sermesant[2,3], Jean-Marc Peyrat[4], Eugene Crystal[1], Sudip Ghate[1], Tommaso Mansi[5], Ilan Lashevsky[1], Beiping Qiang[1], Elliot R. McVeigh[6], Nicholas Ayache[2], and Graham A. Wright[1]

[1] Sunnybrook Research Institute, Univ. of Toronto, Canada
[2] INRIA (Sophia-Antipolis), France
[3] Div. Imaging Science, KCL, London, UK
[4] Siemens Molecular Imaging, Oxford, UK
[5] Siemens Corporate Research, Princeton, NJ, USA
[6] Johns Hopkins University, Baltimore, USA
mihaela.pop@utoronto.ca, gawright@sri.utoronto.ca

Abstract. The aim of this work was to develop a simple and fast 3D MRI-based computer model of arrhythmia inducibility in porcine hearts with chronic infarct scar, and to further validate it using electrophysiology (EP) measures obtained in-vivo. The heart model was built from MRI scans (with voxel size smaller than $1mm^3$) and had fiber directions extracted from diffusion tensor DT-MRI. We used a macroscopic model that calculates the propagation of action potential (AP) after application of a train of stimuli, with location and timing replicating precisely the stimulation protocol used in the in-vivo EP study. Simulation results were performed for two infarct hearts: one with non-inducible and the other with inducible ventricular tachycardia (VT), successfully predicting the study outcome like in the in-vivo cases; for the inducible heart, the average predicted VT cycle length was 273ms, compared to a recorded VT of approximately 250ms. We also generated synthetic fibers for each heart and found the associated helix angle whose transmural variation (in healthy zones) from endo- to epicardium gave the smallest difference (i.e., approx. 41°) when compared to the helix angle corresponding to fibers from DW-MRI. Mean differences between activation times computed using DT-MRI fibers and using synthetic fibers for the two hearts were 6 ms and 11 ms, respectively.

Keywords: electrophysiology, computer modelling, cardiac MR imaging.

1 Introduction

Abnormal heart rhythms are often associated with infarct scars and are a major cause (>85%) of sudden cardiac death [1]. One dangerous manifestation is ventricular tachycardia (VT), where a "reentry circuit" facilitates an abnormal re-excitation of the tissue. In such cases, the electrical wave (i.e., the action potential, AP) loops fast around the scar and through a channel which contains viable bundles of muscle

D.N. Metaxas and L. Axel (Eds.): FIMH 2011, LNCS 6666, pp. 195–205, 2011.

interdigitated within nonconductive collagen [2]. Should the VT circuit fails to be interrupted (e.g., via RF ablation lesions placed onto this channel), the abnormal propagation degenerates into lethal fibrillation, VF. The arrhythmogenic substrate is often located at the border zone (BZ) of the scar and is identified during a clinical electrophysiology (EP) study. The EP study uses surface measurements via invasive catheters and aggressive stimulation protocols to induce VT. More-over, many patients are hemo-dynamically unstable and the inducibility of VT can not be performed in the EP laboratory; thus, the substrate is difficult to identify and to ablate [1]. To complement the EP study in identifying the potential VT patients, 3D non-invasive imaging modalities (e.g., MRI) and computer modelling could be exploited. Several groups have shown that MRI can provide good characterization of the VT substrate by using contrast methods (i.e., delayed-enhanced DE-MRI) [3]. However, the in-vivo voxel size currently used in DE-MRI clinical studies suffers from partial volume effects that might affect the accuracy of the substrate identification, thus higher resolution is desirable.

Computer modelling is a valuable tool used in cardiac EP to understand the normal electrical activity and abnormal propagation of action potential (AP) waves [4]. Considerable efforts have been made by the cardiac computational community to develop multi-scale models (from molecular to tissue level), integrating micro-structures and biophysical details into complex models [5, 6]. Several groups recently worked on developing MRI-based models suitable EP studies. One group [7] has focused on developing virtual models for mouse, rabbit, dog and human hearts from diffusion weighted DW-MRI scans, and further used them in combination with detailed, ionic equations to study VT inducibility, but their study lacked any EP experimental validation. Other researchers focused on using fast eikonal models, which can be attractive for patient-specific applications using clinical cardiac MRI models [8] but are not adequate for modelling reentry (since this model lacks the repolarization phase of AP wave); in addition, they used fibers from atlases which have unclear impact on the accuracy of computed activation times. On the other side, simple macroscopic formalisms based on two-variable equations [9] could be used to model re-entrant waves [10, 11]. We chose to explore this mathematical model, as well as to develop pre-clinical animal models to validate computations that would replicate exactly the in-vivo EP experiments.

The specific aim of this paper was to use a 3D MRI-based model together with a simple macroscopic formalism, to study VT inducibility in infarct hearts. For this, we used our recently developed experimental model in swine with chronic infarct hearts [12]. Here, we perform: i) the construction of the 3D MRI-based model (integrating anatomy, scar extent and fiber directions from DW-MRI); ii) the simulation of VT inducibility (replicating exactly the EP experiment); and iii) comparison of model predictions with those observed during the in-vivo EP study. Figure 1 illustrates the workflow of the current study.

Finally, to study the influence of anisotropy on VT inducibility, we generated synthetic datasets by allowing the helix angle to vary within a wide range (between epi- and endocardium). We then performed simulations with the synthetic dataset for which we found the smallest difference between the helix angle corresponding to synthetic fibers and to the fibers from DT-MRI.

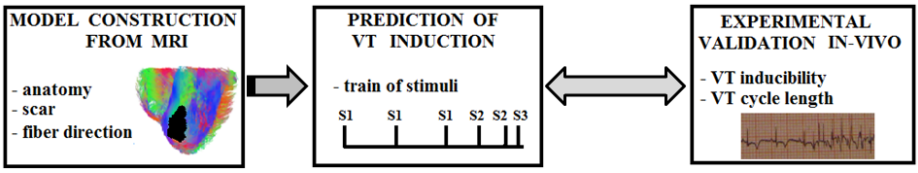

Fig. 1. Diagram of the comparison between the computer model output and in-vivo EP experiments

2 Methodology

2.1 Electrophysiology Study

Myocardial infarction was generated in a swine model by a 90'-min coronary artery occlusion, followed by reperfusion (to create potentially heterogeneous infarct areas), in accordance to the animal protocol approved by our research centre [12]. In this current paper, we focused on two cases in which VT induction was performed: one animal had the left anterior descending (LAD) artery occluded (as shown in Fig. 2a, where the white arrow indicates the occluding balloon), while the other one had the left circumflex (LCX) artery occluded. The in-vivo EP studies were performed at 4-5 weeks post-occlusion and involved the inducibility of VT by following a precise stimulation protocol. This protocol employed the application of a train of stimuli S1 that paced the heart fast (to override the sinus rhythm SNR), followed by several S2-S3 extra stimuli, delivered from the tip of a catheter inserted into the apex of the right ventricle RV (Fig. 2b). The ECG waves were recorded on a paper (allowing us to calculate the resulting VT cycle length when VT was induced).

2.2 Construction of the 3D MRI-Based Computer Model of the Heart

At the completion of the in-vivo EP study, the hearts were explanted, preserved in formalin for few days, and then MR-imaged for anatomy, scar characterization and myocardial fiber directions, using the diffusion weighted DW-MR pulse sequence described in [13]. The MR parameters were given in our previous EP studies [12, 14], together with the methodology regarding the construction of the 3D model from

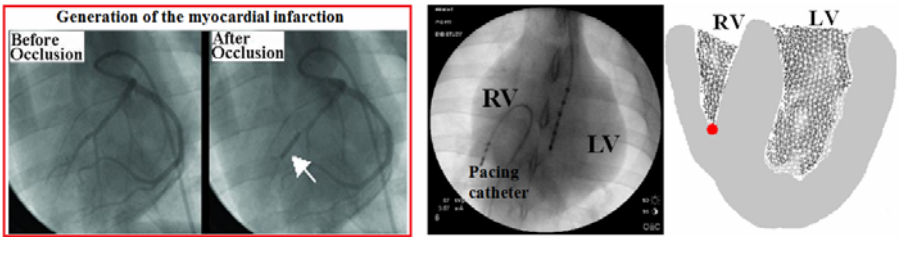

(a) (b) (c)

Fig. 2. Generation of LAD-infarct (a); EP catheters viewed under fluoroscopy (b); and the stimulation point (red dot) in the model, with location corresponding to the catheter tip (c)

apparent diffusion coefficient (ADC) maps, which were next used to segment the heart into three zones: healthy tissue, BZ and infarct scar. Surface meshes were then created for each heart from the 3D anatomy MR scan, and volumetric tetrahedral meshes were generated with TetGen package. Lastly, for each heart, several datasets of synthetic fibers were computer-generated, allowing large transmural variations of fiber direction, such that the helix (inclination) angle from endocardium to epicardium varied on a large range (each from 30º to 90º, with a 5º increment). The calculations of fiber directions and helix angle were performed with Matlab.

2.3 Mathematical Model

We used the macroscopic model developed by Aliev and Panfilov, which is simple, fast, and is based on reaction-diffusion type of equations [8]. In the system of equations given in (1-2) we solve for the action potential (V) and the recovery variable contribution (r) using the Finite Element Method, with an explicit Euler time integration scheme. The term $-kV(V-a)(V-1)$ controls the fast processes (initiation and upstroke of action potential) via the threshold parameter a, while r, determines the dynamics of the repolarization phase.

$$\frac{\partial V}{\partial t} = \nabla \cdot (D\nabla V) - kV(V-a)(V-1) - rV \tag{1}$$

$$\frac{\partial r}{\partial t} = -(\varepsilon + \frac{\mu_1 r}{\mu_2 + V})(ku(u-a-1)+r)\,. \tag{2}$$

This simple model accounts for the heart anisotropy via the diffusion tensor D (which also depends on tissue 'bulk' conductivity d). For instance, the value in the anisotropy ratio is set to 0.14 for a wave propagating almost 2.7 times as fast along the fiber as in the transverse direction. The input values for model parameters were taken from our recent optical fluorescence imaging study performed in infarct hearts [14], and these values were assigned per zone (i.e., infarct, BZ and healthy) and are given in Table 1. Specifically, the values for a (tuning the duration of AP), k (tuning the up-stroke of AP) and the normalized conductivity d were set as in Table 1 (note that a and k values in the scar zone are similarly set like those for BZ, but are in fact irrelevant because the scar is unexcitable, thus d is to 0 (i.e., the AP wave does not propagate through the scar).

Table 1. Electrophysiological parameters in the mathematical model (assigned per zone)

Zone	Parameters		
	a (adimensional)	*k (adimensional)*	*d*
Healthy myocardium	0.112	8	3
Border zone (BZ)	0.2	2	1
Scar (dense)	0.2	2	0

The heart stimulation in the computer model was achieved as follows: i) the sinus rhythm was simulated by applying a square pulse of maximum amplitude (i.e., $V = 1$ since the model output has normalized values for AP) and of 5 ms duration, on both endocardial surface of RV and LV (to mimic Purkinje activation); and, ii) the pacing was simulated by applying a combination of stimuli S1-S2(-S3). These were square pulses 5 ms in duration, of maximum amplitude (i.e., $V = 1$) replicating precisely the stimuli duration and timing like in the EP study, as well as the location of the pacing catheter (at the apex of the RV-endocardium, indicated by the red dot in Fig 2c).

3 Results

3.1 Assessment of VT Inducibility in the EP Study

During the EP experiments, the LCX-infarct heart had non-inducible VT after thirteen pacing stimuli S1 = 550 ms, followed by two S2 extra stimuli at 400 ms and one S3 at 300 ms (thus, S2-S3 coupling interval was 100ms). S3 failed to induce VT, and, consequently, the sinus rhythm was recorded after that (Fig 3a). For the LAD-infarct heart the VT was induced after pacing with eight stimuli S1 = 800 ms, followed by three S2 extra stimuli at 300 ms which induced VT; several VT cycles were recorded, of approximately 250 ms length (Fig 3b).

3.2 Assessment of VT Inducibility in the 3D MR Image-Based Model

Figure 4 shows the results obtained in the LVX-infarct heart, illustrating the construction and parametrization of the 3D MRI-based computer model, together with an example of theoretical propagation of AP wave computed for this heart with non-inducible VT. Specifically, the left panel shows an example of ADC map (2D axial view through the heart) with elevated values of ADC in the scar area, together with the fibers from DT-MRI (with notable severe fibers' disarray in the scar zone). The 3D conductivity map corresponding to the MRI-based model is also illustrated (note that d is set to zero in the scar zone shown in black, and has reduced values in the BZ, as per the input values given in Table 1). The input model parameters also resulted in different EP characteristics for AP wave per zones, for instance: i) the AP duration at 90% recovery is 320 ms for healthy tissue and 275 ms for BZ (as measured in [14]); and ii)

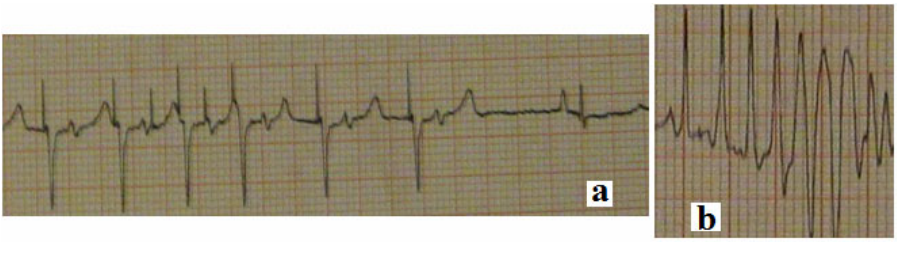

Fig. 3. Non-inducible VT in the LCX-infarct heart, ECG waves recorded at 25 mm/s (a); and inducible VT in the LAD-infarct heart (ECG waves recorded at 10 mm/s), with resulting mean VT cycle length of 250ms (b)

the AP wave has reduced amplitude in BZ (only 0.9) and a slower up-stroke speed compared to the AP wave in the healthy zone. The right panel of Fig. 4 presents simulated activation maps; illustrated are isochronal maps of depolarization times for sinus rhythm (SNR) and following paced cycle (S1), as well as computed all AP waves.

All 3D heart images in Fig. 4 are in presented in a lateral-posterior view.

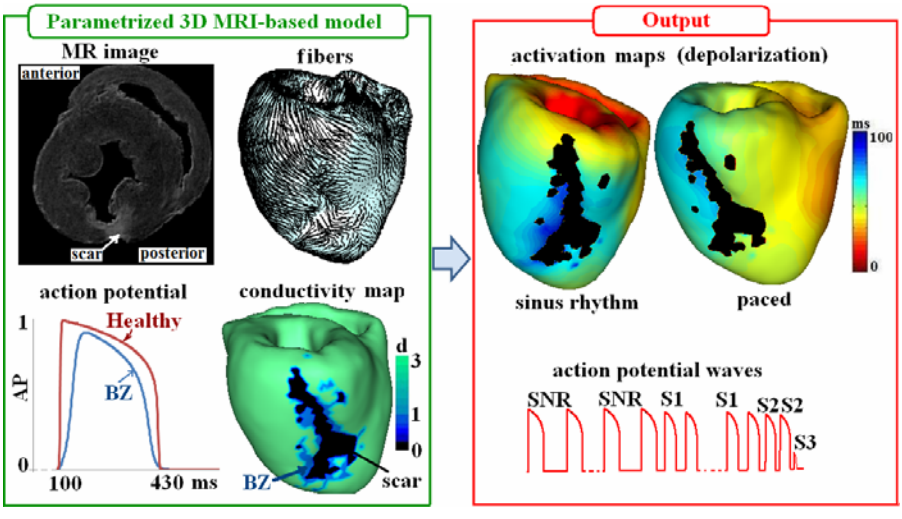

Fig. 4. *Left panel*: The 3D MRI-based parametrized model for the LCX-infarct heart (from segmented ADC maps, and fibers from DT-MRI), together with input 3D conductivity map (with scar in black, healthy in green, BZ in light-blue) and corresponding AP waves (with smaller AP amplitude and shorter duration in the BZ than in the healthy zone). *Right panel*: simulated isochronal maps (depolarization times, with color scale corresponding to early activation times in red and late activation times in blue) during SNR & pacing, and computed AP waves before and after the application of S1-S2-S3 train (resulting in non-inducible VT).

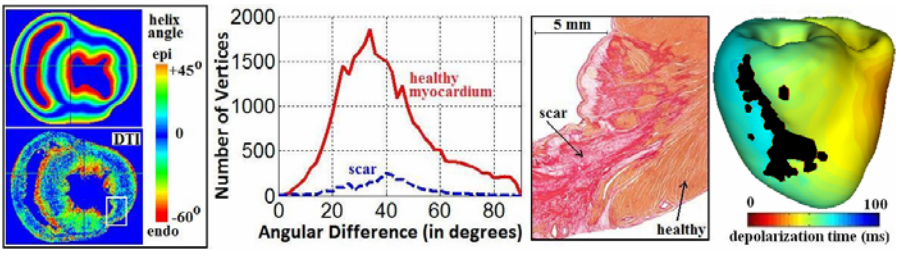

(a) (b) (c) (d)

Fig. 5. Effect of fiber architecture in the LCX-infarct heart: (a) computed helix angle (in a short-axis view) corresponding to synthetic fibers (up) and fibers from DTI (bottom); (b) histogram of angular difference plotted over the vertices in the heart mesh; (c) histological sample taken from the scar area; and (d) and isochronal map of depolarization times during S1 pacing, computed using the synthetic fibers (color scale as in Fig. 4)

Figure 5 shows an example from the results obtained by computer generated synthetic fibers, for which the helix angle varied from +45° on the epicardium to -60° on the endocardium the for LCX-heart. This dataset gave the smallest angular difference (mean ± SD) between the helix angle of synthetic and DTI fibers (i.e., 41.7 ± 20.7° in the healthy heart, and 40.7 ± 18.6° in the scar zone, respectively), see figure caption for more details.

Histological image of Picrosirius Red stain (corresponding to the white square selected in Fig 5a), demonstrated collagen deposition in the transmural scar (in red) and alteration in myofibers' architecture (Fig 5c). Figure 5d shows the activation times obtained using this synthetic dataset, which gave us a mean difference value of 6 ms (over all vertices), compared with the activation times obtained for the case in Fig.4.

Figure 6 presents the 3D MRI-based model obtained for the LAD-infarct heart. The same values for *a, k,* and *d* parameters were assigned per zones as for the LCX-heart. The volume of the scar and border zone was significantly larger than for the LCX-infarct hear; the scar geometry and heterogeneity are notable in the conductivity map. These could explain the inducibility of VT in this LAD-heart.

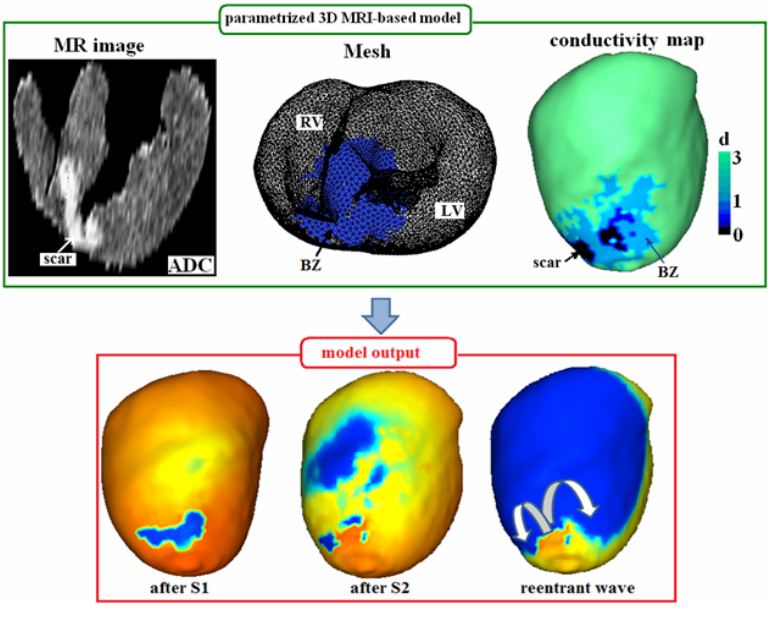

Fig. 6. *Upper panel*: The 3D MRI-based parametrized model for the LAD-infarct heart from segmented ADC maps, together with a top view through the mesh (note the BZ in blue, is visible through the mesh) and the input 3D conductivity map (with *d*-values assigned per zone: with scar in black, healthy in green, BZ in blue). *Lower panel*: simulated isochrones maps (depolarization times) after the S1-S1-S1 train and an extra stimulus S2, resulting in inducible VT and reentrant wave propagating around the scars, in the directions indicated by the white arrows (color scale corresponding to early activation times in red and late activation times in blue).

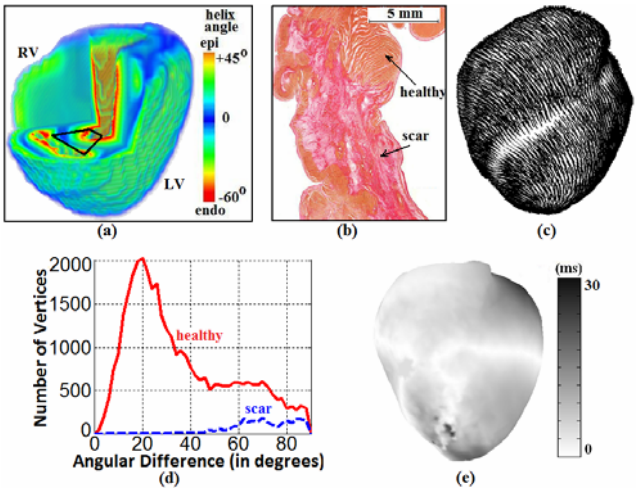

Fig. 7. Effect of fiber architecture in the LAD- heart: (a) computed helix angle (seen through the 3D volume) for synthetic fibers; (b) histological sample take from the septum area indicated by the black rectangle in (a); (c) synthetic fibers displayed on the 3D mesh; (d) histogram of angular difference plotted over the mesh; and (e) absolute difference between activation times computed with DTI-fibers and synthetic fibers (after S1 pacing)

Table 2. Quantitative error analysis associated with differences between activation times computed with DTI fibers and synthetic fibers, respectively

Heart	*r*	RMS-error	mean ± S.D (ms)
LCX-infarct heart	0.97	11.4	6.2 ±4.7
LAD-infarct heart	0.91	22.5	11.1 ± 8.1

Figure 7 shows results obtained for the synthetic fibers generated for LAD-infarct heart. Fig 7a shows the 3D image of the helix angle for the dataset that gave the smallest angular difference (mean ± SD) between this helix angle for synthetic set (with fibers direction shown in Fig 7c) and DTI fibers, that is, 39.8 ± 23.7° in the healthy heart and 64.1 ± 18.5° in the scar zone, respectively (Fig 7d).

Histological image of picrosirius red stain is presented in Fig 7b (for the sample corresponding to the black rectangle selected in the ventricular septum, as seen in Fig 7a). The histopathology demonstrated severe dense collagen deposition and fibers' disarray in the scar area, with islands of viable myocytes at the BZ. Figure 7e shows the absolute difference between computed activation times using DTI fibers and synthetic fibers, and errors indicated in Table 2. Note also that an absolute difference of 12 ms was obtained between the activation times computed during VT using DTI-fibers (with a cycle length of approx 273 ms) and the synthetic fibers (CL of approx 285ms).

Table 2 summarizes the errors associated with the differences between the activation times computed using DTI-fibers and using synthetic fibers (for the dataset that had the helix angle varying from 45° on the epi- to -60° on the endo-cardium). For this comparison, we calculated the Pearson's correlation coefficient (*r*), RMS

error and mean ± S.D. (over the vertices in each heart mesh). Notable is the higher *r* value and a smaller RMS-error and mean difference, for the LCX-infarct heart; we attributed this result to the very small volume of BZ in this heart.

The mesh for the LCX-infarct heart had 212,678 elements, whereas for the LAD-infarct heart the mesh had 245,591 elements. A time step of $5x10^{-5}$s yielded a computational time of 50 min for 1s of simulated heart cycle on a regular PC.

4 Discussion and Future Work

To study the key characteristics of VT potentially observable with non-invasive imaging modalities and to predict VT inducibility, one needs to construct patient-specific models and identify the substrate associated with chronic infarct scars. However, prior to integration into clinical applications, such models have to be properly validated using experiments selected to reflect the electrophysiological phenomena at spatio-temporal scales similar to those considered in simulations.

In summary, in this work we developed and tested a simple and fast 3D MRI-based computer model of arrhythmia inducibility in porcine hearts with chronic infarct scar, and validated it using in-vivo EP measures. Simulation results were performed for two infarct hearts: one with non-inducible and another with inducible VT, successfully predicting the outcome as in the in-vivo EP studies. For the inducible heart the average predicted VT cycle length was slightly longer 273 ms compared to recorded cycle 250 ms, possibly due to model input parameters or simplified global parameterization. A finer tuning could be performed by partitioning the heart in smaller zones as in the optical study presented in [14].

Currently, in our experimental model, we have chosen to use juvenile swine (weighing approximately 40-45kg at the sacrifice time), because they do not have yet M-cells (which account for heterogeneities in AP duration in mature endo-, mid- and epicardial cells). Therefore, our experimental model has simplified restitution properties, with APD constant within the cardiac wall. We thus parameterized the model with constant values for *k, a* and *d* throughout the heart mesh. However, one study limitation is that the values of these parameters were derived from an ex-vivo optical study [14]. Further experimentation is needed to measure restitution properties in-vivo and to customize these model parameters from in-vivo pacing scenarios.

The simulation results obtained with synthetic fibers were encouraging, with rather small differences between activation times. Synthetic fibers are also feasible to use for predicting the VT inducibility. The smallest variation of helix angle between DTI-fibers and synthetic fibers corresponded to a transmural variation of this angle from -60° on endocardium to +45° on epicardium. These values are within ranges reported by other studies performed in sheep, swine and canine hearts [13, 15, 16, 17].

This study used only two hearts, thus further experimentation is needed to fully validate the model. Moreover, to better understand the physical conditions associated with VT inducibility in various reentry circuits, future work will focus on study the influence of scar location, geometry, size and transmurality. Furthermore, we will also focus on building accurate EP models for individual hearts by incorporating in-vivo MR data. For the in-vivo characterization of infarct heterogeneities we can use contrast-agent methods instead of DW-MRI (since the latter is not currently suitable to routine clinical investigations due to image noise and motion, as well as long scans

associated with many directions of gradient diffusion [17]). In a recent MR study performed ex-vivo in porcine hearts with chronic infarct (with voxel size $0.63x0.63x0.6mm^3$), we reported very good agreement between delineation of infarct heterogeneities in MR images obtained using contrast agent method and DW method [18]. This gives us confidence to build, in the future, similar contrast MR-based heart models, and, based on the results of this paper, to use synthetic fibers when DTI data is not available.

References

1. Stevenson, W.G.: Ventricular scars and VT tachycardia. Trans. Am. Clin. Assoc. 120, 403–412 (2009)
2. Ursell, P.C., Gardner, P.I., Albala, A., Fenoglio, J., Wit, A.: Structural and EP changes in the epicardial border zone of canine myocardial infarcts during healing. Circ. Research. 56, 436–451 (1985)
3. Bello, D., Fieno, D.S., Kim, R.J., et al.: Infarct morphology identifies patients with substrate for sustained ventricular tachycardia. J. Am. College of Cardiology 45(7), 1104–1108 (2005)
4. Clayton, R.H., Panfilov, A.V.: A guide to modelling cardiac electrical activity in anatomically detailed ventricles. Progress in Biophysics & Molecular Biology (review) 96(1-3), 19–43 (2008)
5. Hunter, P.J., Crampin, E.J., Nielsen, P.M.: Bioinformatics, multi-scale modeling and the IUPS Physiome project. Brief Bioinform. 9(4), 333–343 (2008)
6. Hunter, P.J., Nielsen, P.M.: A strategy for computational integrative physiology. Physiology 20, 316–325 (2005)
7. Vadakkumpadan, F., Rantner, L., Tice, B., Boyle, P., Prassl, A., Vigmond, E., Plank, G., Trayanova, N.A.: Image-based models of cardiac structure with applications in arrhythmia and defibrillation studies. J. Electrocardiology 42(2), 15 (2009)
8. Chinchapatnam, P., et al.: Model-Based imaging of cardiac apparent conductivity and local conduction velocity for planning of therapy. IEEE Trans. Med. Imaging 27(11), 1631–1642
9. Aliev, R., Panfilov, A.V.: A simple two variables model of cardiac excitation. Chaos, Soliton and Fractals 7(3), 293–301 (1996a)
10. Aliev, R., Panfilov, A.V.: Modeling of heart excitation patterns caused by a local inhomogeneity. Journal of Theoretical Biology 181, 33–40 (1996b)
11. Nash, M.P., Panfilov, A.V.: Electromechanical model of the excitable tissue to study reentrant cardiac arrhythmias. Progress in Biophysics and Molecular Biology 85, 501–510 (2004)
12. Pop, M., Sermesant, M.M., Mansi, T., Crystal, E., Fefer, P., McVeigh, E.R., Dick, A.J., Ayache, N., Wright, G.A.: Characterization of postinfarct scars in porcine models: a combined experimental and theoretical study. In: Ebner, M., O'Neill, M., Ekárt, A., Vanneschi, L., Esparcia-Alcázar, A.I. (eds.) EuroGP 2007. LNCS, vol. 4445, pp. 1–10. Springer, Heidelberg (2007)
13. Helm, P., Tseng, H.J., Younes, L., McVeigh, E.R., Winslow, R.L.: Ex-vivo 3D diffusion tensor imaging and quantification of cardiac laminar structure. Magn. Res. Med. 54, 850–859 (2005)
14. Pop, M., Sermesant, M., Liu, G., Relan, J., Mansi, T., Soong, A., Truong, M., Fefer, P., McVeigh, E.R., Delingette, H., Dick, A., Ayache, N., Wright, G.A.: Construction of 3D MR image-based computer models of pathologic hearts, augmented with histology and optical imaging to characterize the action potential propagation (under revision at Medical Image Analysis (2010)

15. Peyrat, J.-M., Sermesant, M., Delingette, H., Pennec, X., Xu, C., McVeigh, E.R., Ayache, N.: A computational framework for the statistical analysis of cardiac diffusion tensors. IEEE Tran. Medical Imaging 26(11), 1500–1514 (2005)
16. Harrington, K., Rodriguez, F., Cheng, A., Langer, F., Ashikaga, H., Daughters, G., Criscione, J., Ingels, N., Miller, D.: Direct measurement of transmural laminar architecture in the antero-lateral wall of the ovine left ventricles. Am. J. Physiol. Heart Circ. Physiol. 288(3), H1324 (2005)
17. Wu, M.T., Tseng, W.Y., Su, M.Y., Chiou, K.R., Reese, T.G., Yang, C.F.: Diffusion tensor MRI mapping of the fiber architecture remodeling in human myocardium after infarction. Circulation 114, 1036–1045 (2006)
18. Pop, M., Ramanan, V., Yang, Y., Ghugre, N., Qiang, B., McVeigh, E.R., Dick, A., Wright, G.A.: Comparison of scar morphology by 3D multi contrast LE-MRI, 3D DW-MRI and histology in a pig model of chronic infarct. In: Proc. of the 18th ISMRM Conference, Stockholm, Sweden (2010)